Available online at www.sciencedirect.com

SciVerse ScienceDirect

Procedia Computer Science 18 (2013) 1959 – 1968

Procedia Computer Science

International Conference on Computational Science, ICCS 2013

An Offline/Online DDDAS Capability for Self-Aware Aerospace Vehicles

D. Allaire*[a], J. Chambers[b], R. Cowlagi[b], D. Kordonowy[b], M. Lecerf[a], L. Mainini[a], F. Ulker[a], K. Willcox[a]

[a]*Department of Aeronautics and Astronautics, Massachusetts Institute of Technology, Cambridge, MA*
[b]*Aurora Flight Sciences, Cambridge, MA*

Abstract

In this paper we develop initial offline and online capabilities for a self-aware aerospace vehicle. Such a vehicle can dynamically adapt the way it performs missions by gathering information about itself and its surroundings via sensors and responding intelligently. The key challenge to enabling such a self-aware aerospace vehicle is to achieve tasks of dynamically and autonomously sensing, planning, and acting in real time. Our first steps towards achieving this goal are presented here, where we consider the execution of online mapping strategies from sensed data to expected vehicle capability while accounting for uncertainty. Libraries of strain, capability, and maneuever loading are generated offline using vehicle and mission modeling capabilities we have developed in this work. These libraries are used dynamically online as part of a Bayesian classification process for estimating the capability state of the vehicle. Failure probabilities are then computed online for specific maneuvers. We demonstrate our models and methodology on decisions surrounding a standard rate turn maneuver.

Keywords:
DDDAS, data library, Bayesian classification

1. Introduction

A self-aware aerospace vehicle can adapt the way it performs missions by adaptively collecting information about itself and its surroundings and responding accordingly. The vehicle will respond to events and to degradation over time in the same way as a self-aware organism—sprinting when healthy and under favorable conditions, and slowing down as it ages and degrades. There are a number of benefits to enabling such a revolutionary concept. The ability to sense will allow decisions to be made mid-mission. For example, a launch vehicle approaching maximum dynamic pressure can use information regarding current system health to compensate underperforming systems with healthier systems. Under off-nominal conditions or health states, modifications to the mission or flight planning can be implemented to perform the mission based on responsive adaptation by the vehicle to its state. For an aging aircraft that must operate for twenty, thirty, or even fifty years, the ability to tailor or restructure its everyday flight to minimize wear, fatigue, or environmental degradation adds years to its life and reduces the maintenance required to keep the aircraft flight-worthy. Additionally, the aircraft will fly to its capability, performing missions beyond its traditional design envelope.

Email address: dallaire@mit.edu (D. Allaire*)

Selection and peer review under responsibility of the organizers of the 2013 International Conference on Computational Science
doi:10.1016/j.procs.2013.05.365

One of the key challenges to enabling such a self-aware aerospace vehicle is to achieve tasks of dynamically and autonomously sensing, planning, and acting in real time. Our first steps towards achieving this goal are presented here, where we consider the execution of online mapping strategies from sensed strain data to expected vehicle capability while accounting for uncertainty. We consider this task in a novel manner by using available sensor data coupled with a Bayesian classification process as a surrogate for performing expensive statistical inverse calculations. We thus avoid the need to estimate the strain field to use as input to a forward modeling process for estimating vehicle capability through a data-driven reduced order modeling process. The mapping process from strain data to vehicle capability is built with libraries of strain, capability, and maneuever loading that are generated offline using vehicle and mission modeling capabilities we have developed in this work. Online failure probabilities can then be calculated to support decision-making regarding upcoming mission maneuvers.

This paper presents our initial work towards an offline/online DDDAS approach that incorporates data-driven methods in place of traditional inversion methods. To demonstrate our methodology, we have developed a baseline unmanned aerial vehicle (UAV) and detailed models for a structurally significant panel on the wing of the UAV. We discuss the vehicle and the panel in Section 2. In Section 3 we discuss our mission planning capabilities and in Section 4 we demonstrate for a case of three possible damage states, our offline/online DDDAS capability. We provide concluding remarks in Section 5.

2. Modeling Capabilities

In this section we discuss the modeling capabilities we have developed. We first discuss a baseline UAV concept and the bending and shear loads on the wing of the vehicle in a sustained standard rate turn. We then discuss the composite panel and damage models for that panel. The composite panel is used in this work as a surrogate for the complete vehicle in the development of our methodologies.

2.1. Baseline UAV Concept

A conceptual design of a UAV was established to allow for the assessment of structural damage and degradation cases on realistic maneuvers from a vehicle. The design was completed using a first-principles sizing routine [1] and FAR 23 guidelines. As shown in Figure 1, the vehicle has a wing span of 55 feet. It is estimated to cruise at 140

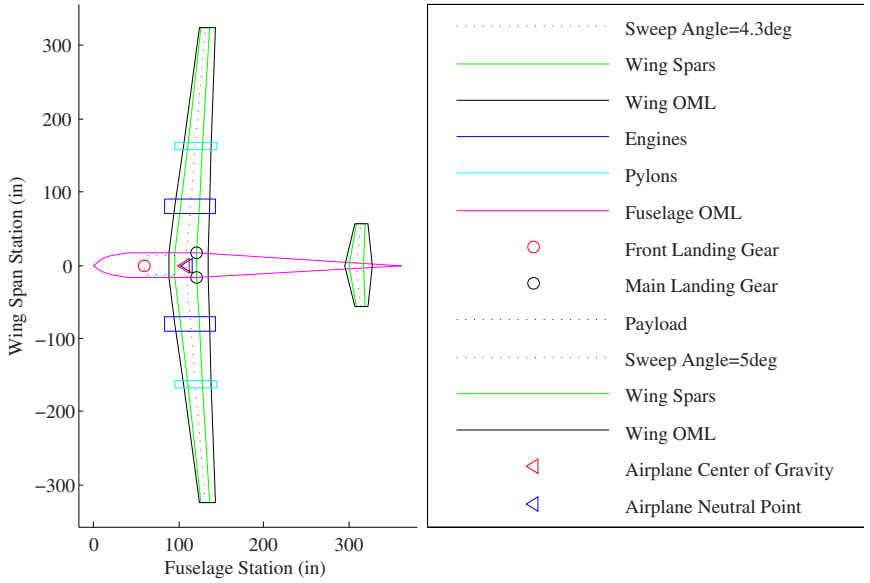

Figure 1. A realistic concept unmanned aerial vehicle established in order to estimate the effect of structural change on capability.

knots (72 m/s) at an altitude of 25,000 ft. A payload of 500 lbs is allowed for in the fuselage. The range of the aircraft

is estimated to be roughly 2500 nmi, corresponding to a duration of 17.5 hours allowing for adequate operational capability to explore maneuverability as a function of the changing structural state of the vehicle.

For this initial assessment of models and algorithms, the concept UAV is to perform a standard rate turn. A sustained standard rate turn is performed by the aircraft by banking at an angle α and increasing the lift normal to the wing planform necessary balance the aircraft weight. This increase in lift creates a net centripetal force component perpendicular to the velocity of the aircraft that changes the heading of the aircraft at a constant velocity; a larger bank angle allows for a higher rotational speed and a tighter radius of turn while increasing the lift force necessary to keep the aircraft at altitude, as shown in Figure 2.

Figure 2. A vehicle (left to right): a) under steady level flight; and b) performing a standard rate turn. The weight of the aircraft (red arrow) is equal to the vertical component of the total aircraft lift (green arrow). The horizontal component of the total aircraft lift under b) creates a centripetal force, causing the aircraft to perform a turn.

The lift distribution along the wing for varying turn rates and radii is estimated using Schrenk's approximation[2] based on an elliptical and chord-wise estimation of lift. This lift distribution is reacted by the wing box structure of the concept UAV in bending and shear. The wing skins (cap) react the majority of the bending while the spars (web) react the majority of the shear. These load reactions induce tension and compression stress, σ_{cap}, in the lower and upper skins respectively due to bending, which are estimated as

$$\sigma_{cap} = \frac{\mathcal{M}_{\perp}(\eta)\, h_{\max}(\eta)}{2 I_{cap}(\eta)}, \tag{1}$$

where $\mathcal{M}_{\perp}(\eta)$ is the bending moment on the wing at normalized spanwise location η perpendicular to the wing sweep angle, $h_{\max}(\eta)$ is the maximum thickness of the wing at η, and $I_{cap}(\eta)$ is the moment of inertia of the wing skins at η. Shear stress, τ_{web}, is induced in the spars due to the shear loading and is estimated as

$$\tau_{web} = \frac{\mathcal{S}_{\perp}(\eta)}{A_{web}(\eta)} \tag{2}$$

where $\mathcal{S}_{\perp}(\eta)$ is the shear force on the wing at η perpendicular to the wing sweep angle, $A_{web}(\eta)$ is the area of the wing spars at η. These relations allow for estimating the turn rate or radius of the concept UAV based on the capability of the structural components to react the loading.

2.2. Composite Panel and Damage Models

The magnitude of wing loading on the concept UAV is directly related to the turn rate; therefore a section of the wing is used as an example panel on which to test the algorithms developed under the DDDAS program. This allows for damage or degradation that reduces the structural capability of the panel to react a sustained load without failure to directly affect the ability of the concept UAV to perform a standard rate turn.

A section of the wing is chosen outboard along the wing span at a location where the wing skin is sized for strength (further outboard the wing skin is sized by minimum gage or handling loads rather than flight loading), as

shown in Figure 3. At a location roughly 260 inches outboard along the wing, the wing skin consisting of 4 plies of MTM45-1/AS4 carbon composite plain weave fabric in a [45/0/0/45] quasi-isotropic layup is necessary to meet the loading requirements due to FAR 23 design requirements[3], while not exceeding strain design allowable values for the plies. Design allowables were computed by assuming a 5% coefficient of variation on the published mechanical properties[4] and calculating the -3σ value, which corresponds to a 99.86% confidence that the actual value is greater than the allowable value.

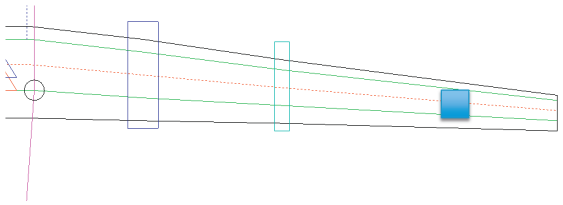

Figure 3. An 18 inch by 18 inch section of the wing upper skin chosen to demonstrate the effect of structural change on capability.

Three structural conditions were initially considered for the example panel: pristine, moderate, and severe damage, as shown in Figure 4. Damage cases are defined as delamination of the first two plies due to low-speed impact on the panel or interlaminar separation caused by stress concentrations under cyclic loading due to embedded foreign object debris or other defects. The panel conditions are modeled using the finite element method and strain values for the panel are estimated for a variety of loading conditions that can be traced back to loading from a variable turn rate. These sets of strains can then be used by the vehicle system to identify the condition of the panel based on measured strain values from strain gauges or other sensors onboard the vehicle. Once the panel condition is determined, the capability of the vehicle to perform a sustained turn necessary to follow a flight path can be determined and a go/no-go decision can be made.

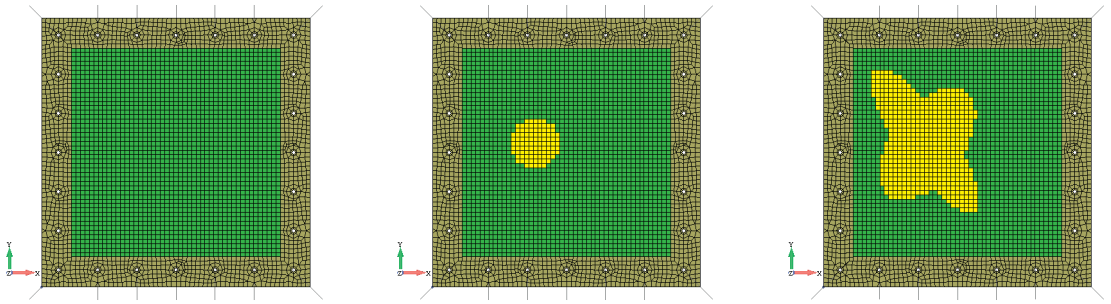

Figure 4. The panel was modeled using the finite element method for three configurations (left to right): pristine; moderate damage; and severe damage. The delamination site for moderate and severe damage are shown in yellow.

The panel is compressively loaded in the Y-axis of Figure 4 with loading that corresponds to a 3.80 load factor on the loads expected when the "air, ground, and water loads are placed in equilibrium with inertia forces[3]" (in this case, steady level flight). This represents the limit maneuvering load factor for a normal category airplane and is the expected design sizing case for the wing. The induced strain in the direction of loading is then estimated using NASTRAN. This directional strain, which puts the fibers in the middle plies of the panel in compression is predicted to be the first failure mode of the panel. A failure index, FI, which is the ratio of expected/predicted load over allowable load, is calculated for this and other failure modes. A failure index of greater than unity predicts an exceedance of the allowed load. When the allowable load is defined by the maximum load sustainable, then a failure index of greater than unity would predict a failure of the panel to sustain the estimated loading. Since materials can have multiple failure modes, multiple failure indices are calculated. The maximum failure index is the envelope of all failure indices calculated, and would represent the first failure mode for the element analyzed.

A load factor of 3.80, which was used for the design of the aircraft, can also describe a reference sustained turn. This load factor can then be used to define a reference radius r and velocity V corresponding to the flight conditions

that would induce a loading that is analyzed by the finite element model. More on this is discussed in Section 3, where mission planning is considered. The predicted strain in the direction of loading for each of the three cases is shown in Figure 5.

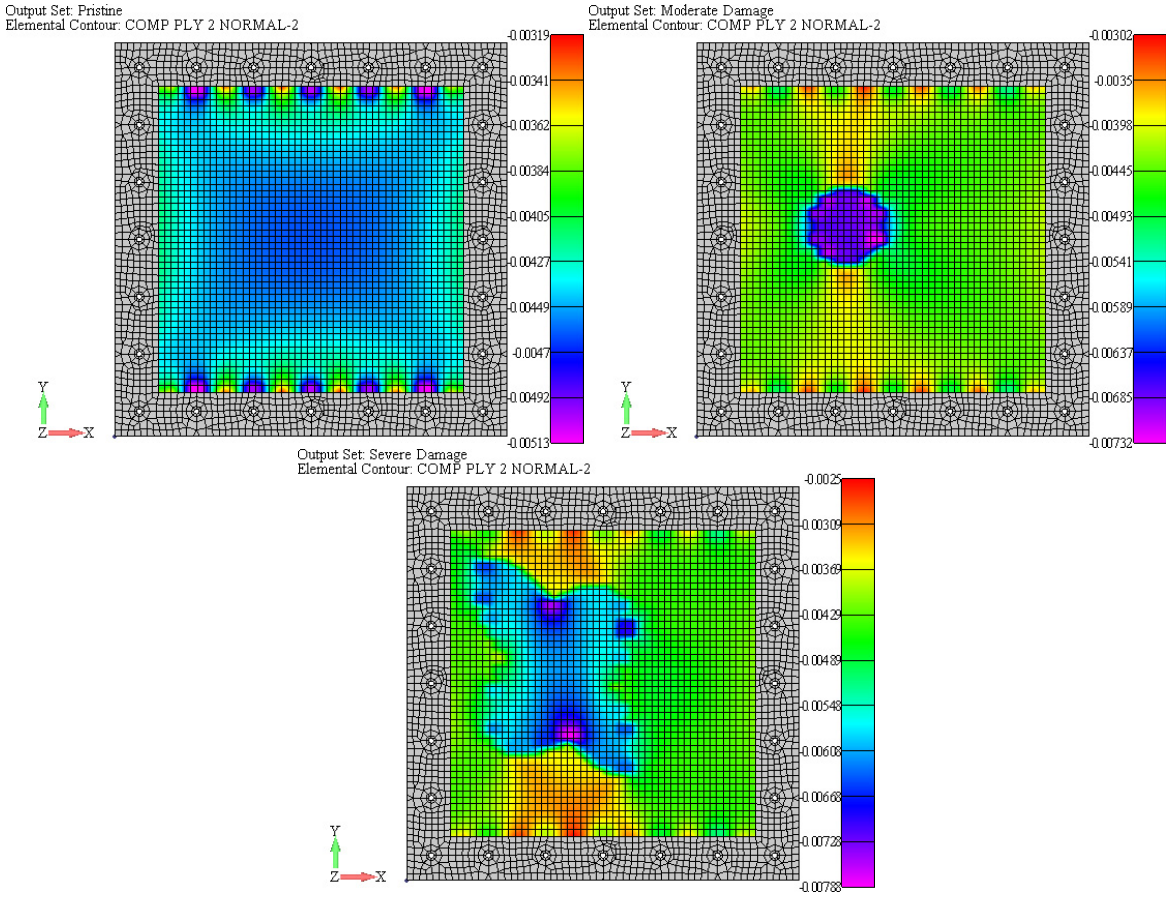

Figure 5. The predicted strain contour in the Y-axis for (left to right): pristine; moderate damage; and severe damage due to Y-axis loading corresponding to the limit maneuvering load factor for a normal category airplane. This load factor corresponds to a reference sustained turn at a specified velocity and resulting turn radius.

The maximum sustainable load factor is calculated in Table 1 by reducing the reference load factor by the maximum calculated failure index. This is a measure of capability, since that is the load factor for which the current condition would cause a maximum failure index of unity (and the predicted loading condition would not exceed the allowable loading). The deterministic minimum turn radius is then calculated for the specified aircraft velocity that induces the maximum load factor.

Table 1. Maximum load factor and corresponding turning radius for the example panel under pristine, moderate and severe damage conditions.

	Pristine	Moderate Damage	Severe Damage
Maximum Failure Index	1.00	1.35	1.45
Reference Load Factor	3.80	3.80	3.80
Velocity (m/s)	72.0	72.0	72.0
Maximum Load Factor	3.80	2.82	2.62
Minimum Radius (m)	144	200	218

We assume in this work that the panel is instrumented at nine equally-spaced locations with strain gauges, as shown in Figure 6. Sensor placement and the development of dynamic sensor data collection techniques are important

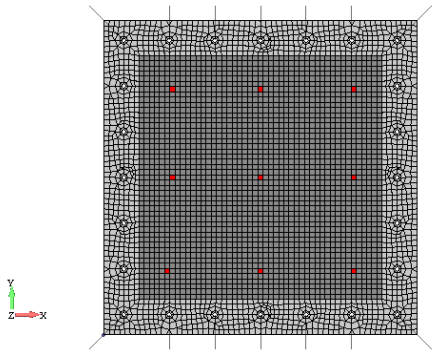

Figure 6. The location of the nine equally-spaced strain gauge sensors on the example panel.

topics of future work not considered here. These strain gauges are oriented in the direction of the load. The predicted strain at the nearest element of the finite element model for each of these locations under the reference load factor is shown in Table 2. The predicted strains scale linearly by the load factor, so that the strains can be estimated for other load factors based on the ratio of the actual load factor to the reference load factor.

Table 2. Strain gauge sensor locations and predicted strain in the direction of loading for pristine, moderate and severe damage cases.

	Location		Pristine	Moderate Damage	Severe Damage
	X (in)	Y (in)		Strain (in/in)	
Sensor 1	3.94	14.36	-0.004411	-0.004378	-0.006177
Sensor 2	9.00	14.06	-0.004296	-0.004133	-0.003354
Sensor 3	14.36	14.06	-0.004442	-0.004487	-0.004496
Sensor 4	3.94	9.00	-0.004409	-0.004485	-0.003979
Sensor 5	9.00	9.00	-0.004618	-0.004900	-0.005028
Sensor 6	14.36	9.00	-0.004376	-0.004316	-0.004401
Sensor 7	3.64	3.64	-0.004451	-0.004356	-0.004049
Sensor 8	9.00	3.64	-0.004273	-0.004073	-0.003185
Sensor 9	14.36	3.64	-0.004429	-0.004449	-0.004493

3. Motion Planning

In this section we discuss our motion planning capability for our demonstration problem. Informally, motion planning for an autonomous vehicle, modeled by a controlled nonlinear dynamical system, refers to the problem of finding admissible control inputs for this dynamical system to drive its states from a pre-specified initial condition to a pre-specified goal [5]. Typically, the motion planning problem involves the notion of a cost that must be minimized along the resultant state trajectory, and the notion of obstacles, which are regions of the state space that any feasible state trajectory must avoid. In addition, the notion of a higher-level mission may be involved, which involves logical specifications on the objective of the motion planning problem. Motion planning algorithms are critical for enabling autonomy in mobile vehicles, such as UAVs.

The objective of this research is to develop capability-aware autonomy for UAVs. The term capability refers to a concise quantitative characterization of the structural health condition of the airframe. Here, we define capability as the maximum allowable load factor (i.e., the ratio of lift to weight) that the aircraft can safely sustain. In the context of motion planning, an upper bound $n_{\max}$ on the load factor, n, is equivalent to a constraint on the minimum radius, $r_{\min}$, of turns that the aircraft can feasibly perform. Specifically, the relation between $r_{\min}$ and $n_{\max}$ is given as [6]:

$$r_{\min} = \frac{V^2}{g\sqrt{n_{\max}^2 - 1}}, \tag{3}$$

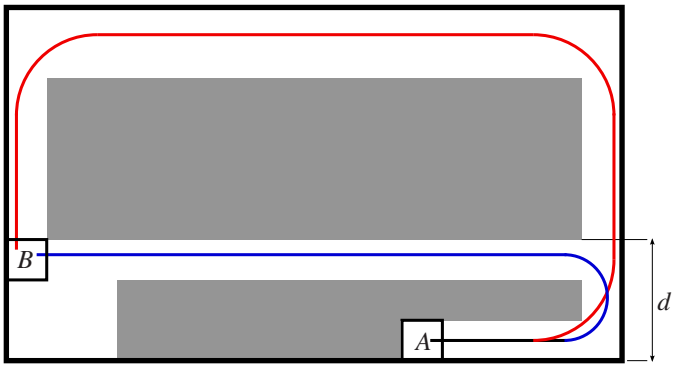

Figure 7. Mission environment for developing DDDAS capabilities for a self-aware UAV.

where V is the airspeed.

As a simple, yet illuminating example of the challenges involved in enabling capability-aware autonomy in UAVs, we consider the environment shown in Fig. 7. Here, A and B denote two regions of interest, and the gray areas denote obstacles. Within this environment, consider a mission informally specified as *"Fly from region A to region B while avoiding all obstacles as quickly as possible."* For the sake of discussion, let $d = 6,000$ m, and suppose that the aircraft flies at a constant airspeed of $v = 350$ knots $= 180.1$ m/s. First suppose that this mission is to be achieved while maintaining the load factor, at all times during the flight, less than or equal to $n_{\max,1} = 2.5$. It follows by Eqn. (3) that the minimum turn radius for the aircraft in this case is $r_{\min,1} = 1,444$ m. Because $2r_{\min,1} < d$, it is easy to see from Fig. 7 that the aircraft can satisfy the mission specifications by following a path similar to the blue-colored path in Fig. 7. Now suppose that this mission is to be achieved while maintaining the load factor, at all times during the flight, less than or equal to $n_{\max,2} = 1.3$. It follows by Eqn. (3) that the minimum turn radius for the aircraft in this case is $r_{\min,2} = 3,978$ m. Here, $2r_{\min,2} > d$, and the aircraft will be unable to follow a path similar to the blue-colored path, and the mission can be satisfied only by following a path similar to the red-colored path in Fig. 7. The upper bounds $n^1_{\max}$ and $n_{\max,2}$ on the load factor are examples of the aircraft's structural capability constraints in possibly two different health states. A capability-aware UAV would be required to plan paths according to the load factor constraints corresponding to different structural health states.

4. Demonstration

In this section we demonstrate our initial work towards offline/online DDDAS capability. The demonstration consists of a decision regarding which mission to fly from point B to point A. In the following subsections we setup the decision problem, discuss the offline libraries of strain, capability, and mission information, provide background on our Bayesian approach to mapping strain data to vehicle capability, and present results.

4.1. Problem Setup

The specific planning problem we consider in this work is, given a set of possible paths from point B to point A in Figure 7, select the shortest path subject to a mission failure probability of less than 0.0001. We also have the option of mission no-go if there is no feasible option. For this problem we do not consider the effects of degradation. Thus, the mission failure probability is based entirely on the maximum load sustained during the mission. Only the composite panel discussed in Section 2.2 is considered in the failure probability estimation. The panel is thus a proxy for the complete vehicle.

4.2. Offline Libraries

As an example of a possible DDDAS path to a self-aware UAV, we consider the offline population of information libraries. These libraries can contain experimental data, model input/output data, expert information, and models themselves. For our demonstration problem here, we consider a strain library, a capability library, and a mission

library. Each is discussed in turn.

Strain Library. The strain library for our example problem consists of strain data generated at 9 different locations on the composite panel as shown previously in Figure 6. This data was generated for each location under a maximum loading condition for the panel in the pristine, moderate, and severe damage cases. The data is presented in Table 2. Online interpolation of this offline generated strain library is used in the demonstration to estimate the probability of the panel being in each damage case. This concept of online interpolation of an offline library is something we will explore in detail in future work. The concept embodies the DDDAS paradigm of leveraging data to support modeling, and in this case, replace modeling entirely.

Capability Library. The capability library for our example problem consists of the load factor for each damage state under the maximum loading condition for the panel in each damage state. The capability data is presented in Table 1. Online this data is used to estimate the failure probability for the standard rate turn maneuver based on the probability of being in each capability state as estimated via the online use of the strain library and acquired strain data.

Mission Library. The mission library for our example problem consists of two possible paths from B to A in Figure 7, as well as an abort option. The two possible paths from B to A are shown in blue (tighter turn) and red. The concept we are demonstrating here is that of generating an offline library of optimal mission plans that can be coupled with online data to drive online mission decision-making. Concepts of mission plan interpolation will be explored in the future, as well as probabilistic extensions to more traditional H-cost motion-planning algorithms [7].

4.3. Data-Driven Mapping from Strain to Capability to Failure Probability

A key aspect of our DDDAS methodology is the ability to rapidly move from sensed data to vehicle state to mission decision-making. To enable this, we consider the online use of our information libraries driven by acquired strain data during a mission. The first step is the estimation of the probability that we are in a particular damage state. We do this by implementing a Bayes classifier under the assumption of independent features, where here the features are the online strain gauge data, which are indepedent conditioned on a loading case. Let the strain gauge data from the nine sensors be represented by a random vector $[G_1|X_j, G_2|X_j, \ldots, G_9|X_j]^T$, where each $G_i|X_j \sim \mathcal{N}(\bar{g}_{i,j}, \sigma_g^2)$ and X_j denotes conditioning on the damage state (pristine, moderate, or severe). Here also, σ_g^2 is the variance, assumed identical, associated with each random variable representing the strain gauge data. The expected value of each of these random variables, $\bar{g}_{i,j}$, is calculated as

$$\bar{g}_{i,j} = g_{i,j,\max} \frac{n}{n_{j,\max}}, \tag{4}$$

where $g_{i,j,\max}$ is the strain gauge output for gauge i under the maximum loading condition, $n_{j,\max}$, for damage state X_j. Let d_i denote the actual output of the ith strain gauge. We may construct a likelihood function, $L(X_j|\mathbf{d})$, where $\mathbf{d} = [d_1, \ldots, d_9]^T$ as

$$L(X_j|\mathbf{d}) = \prod_{i=1}^{9} p_i(d_i|X_j), \tag{5}$$

where $p_i(d_i|X_j)$ is the probability density function of $G_i|X_j \sim \mathcal{N}(\bar{g}_{i,j}, \sigma_g^2)$ evaluated at d_i. If we define prior probabilities for each damage state as $P(X_j)$, then using Bayes rule we arrive at posterior estimates of probability of being in each state, $P(X_j|\mathbf{d})$ as

$$P(X_j|\mathbf{d}) = \frac{P(X_j)L(X_j|\mathbf{d})}{\sum_j P(X_j)L(X_j|\mathbf{d})}. \tag{6}$$

Given our estimates of the probability that we are in each damage state, we can produce estimates of the probability of failure on a given maneuver. We assume that our capability estimates for each damage state have some associated uncertainty due to our inability to perfectly model the physics of the loading on the panel. We capture this by assigning a random variable C_j to the capability in each damage state j. Here we assume that each damage state has a corresponding capability state. However, in future work we will consider possible many to few mappings from a large library of damage states onto a possibly much smaller space of capabilities. We assume each $C_j \sim \mathcal{N}(\bar{c}_j, \sigma_C^2)$, where $\bar{c}_j$ is the load factor associated with the maximum loading condition for damage state j and σ_C^2 is the variance,

assumed identical, associated with each C_j. We also assume in this demonstration that the load, n, on the panel is uncertainty, which could be caused by a number of factors (e.g., environmental conditions). We capture this uncertainty by assuming we can represent the load as a random variable $N \sim \mathcal{N}(\bar{n}, \sigma_N^2)$, where $\bar{n}$ is the nominal load and σ_N^2 is the variance of the random variable N. Then, for a given damage state, the probability of failure, $P_{\text{fail}}|X_j$, on a particular maneuver is $P_{\text{fail}}|X_j = P(\{N - C_j\}) > 0$. The overall probability of failure, P_{fail} is then given as

$$P_{\text{fail}} = \sum_j P(X_j|\mathbf{d}) P_{\text{fail}}|X_j. \tag{7}$$

4.4. Results

We consider here a specific example for the mission scenario shown in Figure 7, where a decision must be made based on current estimated vehicle capability on whether to traverse the blue path (tighter turn), the red path, or to abort the mission of travelling from B to A. We have assumed the numerical quantities in this section primarily to demonstrate some of the potential of such a DDDAS capability aboard a UAV.

As noted in Section 4.1, we wish to travel from B to A as quickly as possible but we require that the probability of mission failure be less than 1×10^{-9}. We assume the aircraft flies at a constant velocity of 72 m/s, and thus, the tighter turn mission will arrive at point A faster than the other option. Therefore, the online information that must be calculated is the feasibility of each path based on estimated capability, which is based on the acquisition of online strain gauge data. We assume that the radius of the tighter turn is 150 meters and that the radius of the wider turn is 230 meteres. For uncertainty information, we assume $\sigma_G^2 = 0.0001, \sigma_C^2 = 0.01$, and $\sigma_N^2 = 0.02$. We consider three cases in turn.

Case 1. For the first case we assume we received the strain gauge data provided in the fourth column of Table 3. We acquired this data by performing a gentle test turn with radius 500 meters to provide some information for identifying our damage state (much the same way a human may inspect him or herself for a broken bone by testing movements and applying pressure in various locations). This concept of dynamically gathering data online via optimal experimental design is something we will consider in more detail in future work. Using Equations 3 and 4, we estimate the load and the expected value of the output of each strain gauge conditioned on each damage state. Note that estimate a deterministic value for $\bar{g}_{i,j}$ by using $\bar{n}$ and $\bar{n}_{i,j,\max}$ in Equation 4, where $\bar{n}_{i,j,\max}$ is the estimated deterministically from Equation 3. Using the acquired data in Table 3, the estimates of $\bar{g}_{i,j}$, and Equation 6, with $P(X_j) = 1/3$ for all j, we estimate the probability of being in each damage state as $P(X_{\text{pristine}}) \approx 1$, $P(X_{\text{moderate}}) \approx 0$, and $P(X_{\text{severe}}) \approx 0$. For the tigher turn we estimate the failure probability given this information as $P_{\text{fail}} = 3.5 \times 10^{-10}$. Thus, for this case, the mission planner selects the tighter turn (blue path) from the mission library as the optimal mission.

Table 3. Measured strain in the direction of loading for three test cases.

	Location		Case 1	Case 2	Case 3
	X (in)	Y (in)		Strain (in/in)	
Sensor 1	3.94	14.36	-0.001697	-0.002282	-0.003388
Sensor 2	9.00	14.06	-0.001485	-0.001930	-0.002030
Sensor 3	14.36	14.06	-0.001691	-0.002541	-0.002450
Sensor 4	3.94	9.00	-0.001684	-0.002091	-0.002331
Sensor 5	9.00	9.00	-0.001842	-0.002494	-0.002786
Sensor 6	14.36	9.00	-0.001679	-0.002127	-0.002379
Sensor 7	3.64	3.64	-0.001681	-0.002414	-0.002216
Sensor 8	9.00	3.64	-0.001593	-0.002160	-0.001660
Sensor 9	14.36	3.64	-0.001733	-0.002323	-0.002395

Case 2. For the second case we assume we performed the 500 meter radius turn and acquired the strain gauge data provided in the fifth column of Table 3. Following the same procedure as in Case 1, we now estimate the probability of being in each damage state as $P(X_{\text{pristine}}) \approx 0$, $P(X_{\text{moderate}}) \approx 1$, and $P(X_{\text{severe}}) \approx 0$. For the tighter turn, we estimate the failure probability given this information as $P_{\text{fail}} \approx 1$. Thus, the tighter turn is not feasible in this case. For the wider turn, we estimate the failure probability given this information as $P_{\text{fail}} 5.8 \times 10^{-34}$. Thus, for this case, the mission planner selects the wider turn from the mission library as the optimal (and in fact only feasible) mission.

Case 3. For the third case we assume we performed the 500 meter radius turn and acquired the strain gauge data provided in the sixth column of Table 3. Following the same procedure as in Case 1 and 2, we now estimate the probability of being in each damage state as $P(X_{\text{pristine}}) \approx 0$, $P(X_{\text{moderate}}) \approx 0$, and $P(X_{\text{severe}}) \approx 1$. For the tighter turn, we estimate the failure probability given this information as $P_{\text{fail}} \approx 1$. Thus, the tighter turn is not feasible in this case either. For the wider turn, we estimate the failure probability given this information as $P_{\text{fail}} 1.6 \times 10^{-7}$. Thus, the wider turn is also not feasible. Since there are no feasible missions in the mission library, the mission planner selects to abort the mission in this case.

5. Conclusions

We have demonstrated an offline/online DDDAS capability that incorporates online data collection as part of a mapping procedure from data to capability state. In our demonstration, the damage states where distinct enough that classification based on strain gauge data (and the assumptions regarding uncertainty) placed the vehicle in a particular damage state with probability near unity for each case tested. By identifying the vehicle's capability state we were able to support online mission re-planning.

This work has opened a number of avenues for future work. The construction of offline information libraries and there online use is a key aspect of developing what is essentially a data-driven reduced-order modeling capability that connects all modeling and decision aspects of the self-aware UAV problem. Optimal online data collection informed by data and modeling needs is another key ingredient that merits future research. For the work presented here in particular, we will in the future compare our DDDAS methodology to more traditional approaches such as solving a statistical inverse problem for the strain field from strain gauge data and then propagating that field forward through offline and online modeling tools to estimate vehicle capability.

References

References

[1] E. Greitzer, P. Bonnefoy, E. De la Rosa Blanco, C. Dorbian, M. Drela, D. Hall, R. Hansman, J. Hileman, R. Liebeck, J. Lovegren, J. P. P. Mody, S. Sato, Z. Spakovszky, C. Tan, J. Hollman, J. Duda, N. Fitzgerald, J. Houghton, J. Kerrebrock, G. Kiwada, D. Kordonowy, J. Parrish, J. Tylko, E. Wen, W. Lord, N+3 aircraft concepts designs and trade studies, final report, volume 2, Nasa cr-2010-216794/vol2, NASA Glenn Research Center, Cleveland, Ohio 44135 (2010).

[2] D. Raymer, Aircraft design : a conceptual approach, American Institute of Aeronautics and Astronautics, Reston, Va, 2006.

[3] Federal aviation regulations, part 23, title 14, Code of Federal Regulations (1999).

[4] Umeco mtm451- high service temperature, flexible cure, vacuum processable prepreg system product data sheet, pDS1205/03.12/7b (2012).

[5] H. Choset, K. Lynch, S. Hutchinson, G. Kantor, W. Burgard, L. Kavraki, S. Thrun, Principles of Robot Motion: Theory, Algorithms, and Implementations, The MIT Press, 2005.

[6] J. D. Anderson, Aircraft Performance and Design, McGraw-Hill, Boston, MA, USA., 1999.

[7] R. V. Cowlagi, P. Tsiotras, Hierarchical motion planning with dynamical feasibility guarantees for mobile robotic vehicles, IEEE Transactions on Robotics 28 (2) (2012) 379 – 395.